

Magnetochemistry 2015, 1, 45-61; doi:10.3390/magnetochemistry1010045

OPEN ACCESS

**magnetochemistry**

ISSN 2312-7481

[www.mdpi.com/journal/magnetochemistry](http://www.mdpi.com/journal/magnetochemistry)

Article

## Novel Topologies in Vanadium-*bis*- $\beta$ -Diketone Chemistry: A [V<sub>4</sub>] and a [V<sub>6</sub>] Metallacyclophane

Ivana Borilovic <sup>1</sup>, Olivier Roubeau <sup>2</sup>, Irene Fernández Vidal <sup>3</sup>, Simon J. Teat <sup>4</sup> and Guillem Aromí <sup>1,\*</sup>

<sup>1</sup> Departament de Química Inorgànica, Universitat de Barcelona, Diagonal 645, Barcelona 08028, Spain; E-Mail: ivana.borilovic@qi.ub.es

<sup>2</sup> Instituto de Ciencia de Materiales de Aragón (ICMA), CSIC and Universidad de Zaragoza, Plaza San Francisco s/n, Zaragoza 50009, Spain; E-Mail: roubeau@unizar.es

<sup>3</sup> Unitat d'Espectrometria de Masses de Caracterització Molecular, CCiT, Universitat de Barcelona, Martí i Franqués 1-11, Barcelona 08028, Spain; E-Mail: i.fernandez@ub.edu

<sup>4</sup> Advanced Light Source, Berkeley Laboratory, 1 Cyclotron Road, MS2-400, Berkeley, CA 94720, USA; E-Mail: sjteat@lbl.gov

\* Author to whom correspondence should be addressed; E-Mail: guillem.aromi@qi.ub.es; Tel.: +34-9-3403-9760.

Academic Editor: Carlos J. Gómez García

Received: 2 October 2015 / Accepted: 18 November 2015 / Published: 2 December 2015

**Abstract:** Exploring the chemistry of vanadyl ions (VO<sup>2+</sup>) with *bis*- $\beta$ -diketone ligands, in pyridine reactions of vanadyl sulfate with 1,3-*bis*-(3-oxo-3-(2-hydroxyphenyl)-propionyl)-benzene (H<sub>4</sub>L1) and 1,3-*bis*-(3-oxo-3-(2-hydroxyphenyl)-propionyl)-pyridine (H<sub>4</sub>L2), two novel clusters, [(V<sup>IV</sup>O)<sub>4</sub>(H<sub>2</sub>L1)<sub>4</sub>(py)<sub>4</sub>] (**1**) and [(V<sup>V</sup>O)<sub>4</sub>(V<sup>IV</sup>O)<sub>2</sub>(O)<sub>4</sub>(L2)<sub>2</sub>(py)<sub>6</sub>] (**2**) were prepared and characterized. Due to the conformational flexibility of the ligands, both entities exhibit very peculiar metal topologies and composition, differing significantly from structural patterns established in the related chemistry of divalent 3d metals. Structural analysis also unveils the existence of the most complex metallamacrocycles from this family to date. Studies of the magnetic properties via bulk magnetization measurements and EPR spectroscopy confirmed the existence of uncoupled long-distant S = 1/2 metal centers and the spin ground states S = 2 and S = 1 of the clusters.

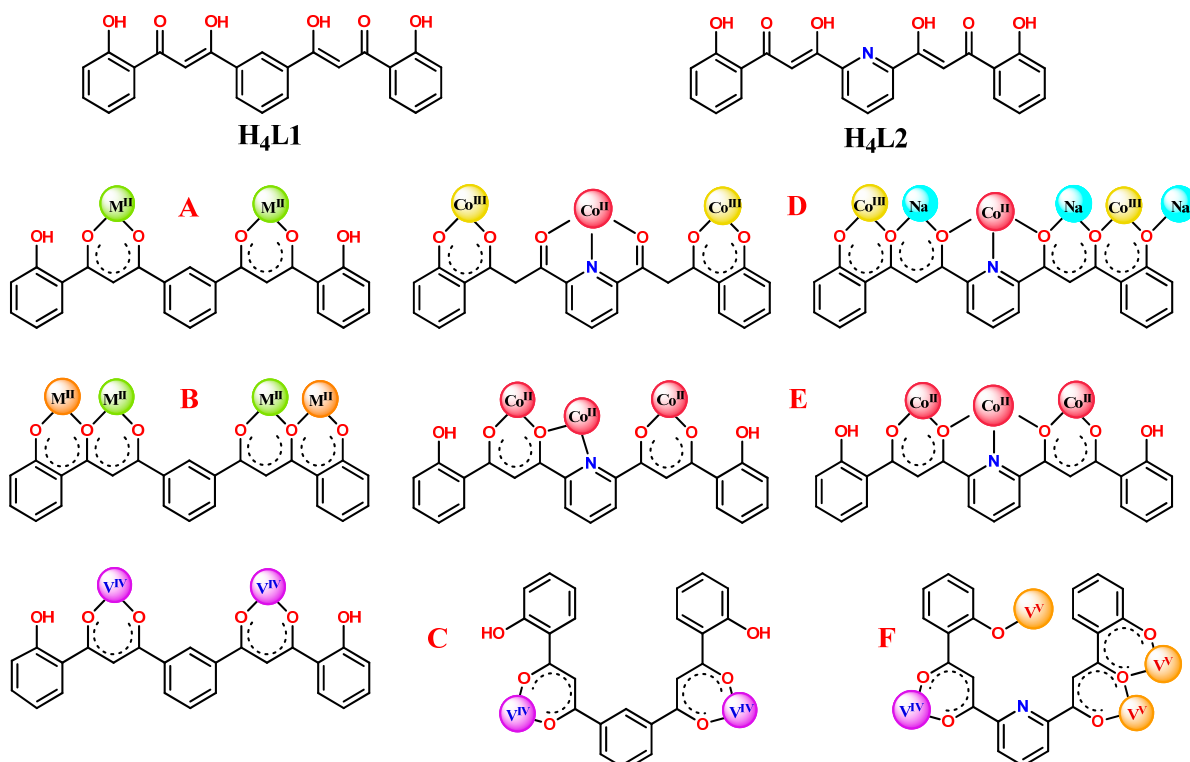
**Keywords:** vanadyl clusters; poly- $\beta$ -diketone ligands; magnetic properties; self-assembly; metallamacrocycles

## 1. Introduction

The field of molecular magnetism has illuminated the discovery of magnetic functional systems of molecular bases, such as single molecule magnets (SMMs) [1–5], bi-stable spin crossover (SCO) materials [6–8], or proposed molecular hardware for spin-based quantum computing (QC) [9–12]. In this endeavor, the field of coordination chemistry is an inexhaustible spring of tools resulting from the combination of versatile organic scaffolds and the diverse physico-chemical properties of transition and rare-earth metals. In this context, the implementation of judiciously engineered ligands, such as *bis*- $\beta$ -diketones [13], has allowed the preparation of abundant families of metallohelicates [14–16], linear molecular platforms [17,18], weakly coupled molecular cluster pairs [19,20], metallamacrocycles [21–24], and cage clusters [25–28] displaying interesting topologies and unprecedented structural features. However, despite that the vast majority of their coordination entities involve divalent and trivalent 3d metal ions, the chemistry of *bis*- $\beta$ -diketone ligands with vanadium remains relatively scarce, especially when considering the diverse reactivity of this metal together with the biological and catalytic importance of its compounds [29–34]. To date, very few vanadium metallo-organic structures of *bis*- $\beta$ -diketones have been reported. These include one dinuclear V<sup>III</sup> helicate [14] and a collection of dinuclear metallamacrocyclic compounds of V(II), V(III), and V(IV) [22,35,36]. Nevertheless, the importance of vanadium in emerging areas of molecular magnetism is increasing. In fact, one of the first 3d coordination clusters identified as SMM was a [V(III)<sub>4</sub>] “butterfly” complex [37]. In addition, one of the first complexes exhibiting long quantum coherence, revealed through the observation of Rabi oscillations, as a prerequisite for the quantum manipulation of the spin was a [V(IV)<sub>15</sub>] cluster [38]. In this line, electrically gating the interaction between two (VO<sub>2</sub>)<sup>2+</sup> groups at the ends of a polyoxometallate was proven theoretically to enable the realization of a quantum gate [38]. More recently, the quantum coherence of the EPR transitions between the electronuclear states within a mononuclear V(IV) complex were described as an important resource for the quantum processing of information [39].

Here, we show the unusual coordination chemistry of vanadyl ions VO<sup>2+</sup> with two *bis*- $\beta$ -diketone ligands (Scheme 1), 1,3-*bis*-(3-oxo-3-(2-hydroxyphenyl)-propionyl)-benzene (H<sub>4</sub>L1) and 1,3-*bis*-(3-oxo-3-(2-hydroxyphenyl)-propionyl)-pyridine (H<sub>4</sub>L2), designed and prepared in our group [40,41]. Prior to this work, ligand H<sub>4</sub>L1 was employed in the synthesis of dinuclear and (homo- or heterometallic) tetranuclear complexes of 3d transition metals containing linear [M<sub>2</sub>(H<sub>2</sub>L1)<sub>2</sub>] [40] and [M<sub>4</sub>(L1)<sub>2</sub>] [19,42] central cores. On the other hand, ligand H<sub>4</sub>L2 has been used exclusively in preparation of Co(II) coordination compounds with some unprecedented features. Employment of the ligand under weakly basic conditions allowed deprotonating only the  $\beta$ -diketone moiety leading to the octanuclear cluster [Co<sub>8</sub>O(OH)(H<sub>2</sub>L2)<sub>6</sub>]NO<sub>3</sub>, which encapsulates a very rare [ $\mu_3$ -O···H··· $\mu_3$ -O] structural motif [27]. The use of a strong base (TBAOH, NaH) and a coordinating solvent (pyridine) directed the outcome of aerobic analogous reactions towards the unusual tetranuclear [Co<sub>4</sub>(L2)<sub>2</sub>(OH)(py)<sub>7</sub>]NO<sub>3</sub> and octanuclear [Co<sub>8</sub>Na<sub>4</sub>(L2)<sub>4</sub>(OH)<sub>2</sub>(CO<sub>3</sub>)<sub>2</sub>(py)<sub>10</sub>](BF<sub>4</sub>)<sub>2</sub> coordination

compounds [28]. The exceptionality of these structures lies in the existence of a very rare bridging “crevice” pyridine ligand within the former, or two trapped carbonate anions, within the latter, forced to stay at the shortest non-covalent distance ever observed. Given the structural versatility of H<sub>4</sub>L1 and H<sub>4</sub>L2, we decided to explore their potential for organizing the vanadyl ion (VO<sup>2+</sup>) within molecular assemblies with the long-term view of exploiting its potential in the context of quantum computing. Thus, the tetranuclear neutral cluster [(VO)<sub>4</sub>(H<sub>2</sub>L1)<sub>4</sub>(py)<sub>4</sub>] (**1**) was obtained with ligand H<sub>4</sub>L1, which exhibits a combination of linear and bent (V-shaped) conformations (Scheme 1) favoring the formation of a grid-like coordination cage. On the other hand, H<sub>4</sub>L2 yields the mixed valence V<sup>V</sup>V<sup>IV</sup> neutral cluster [(V<sup>V</sup>O)<sub>4</sub>(V<sup>IV</sup>O)<sub>2</sub>(O)<sub>4</sub>(L2)<sub>2</sub>(py)<sub>6</sub>] (**2**), with a radically different structure, resulting from an unprecedented coordination mode for this ligand (Scheme 1).



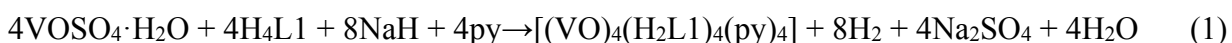
**Scheme 1.** Ligands H<sub>4</sub>L1 and H<sub>4</sub>L2, together with their coordination modes and conformations seen in previous reports and in compounds **1** and **2**. (A) [M<sub>2</sub>(H<sub>2</sub>L1)<sub>2</sub>] [40]; (B) [M<sub>4</sub>(L1)<sub>2</sub>] and [M<sub>2</sub>M'<sub>2</sub>(L1)<sub>2</sub>] [19,42]; (C) [(VO)<sub>4</sub>(H<sub>2</sub>L1)<sub>4</sub>(py)<sub>4</sub>] (**1**); (D) [Co<sub>4</sub>(L2)<sub>2</sub>(OH)(py)<sub>7</sub>]NO<sub>3</sub> (**left**) and [Co<sub>8</sub>Na<sub>4</sub>(L2)<sub>4</sub>(OH)<sub>2</sub>(CO<sub>3</sub>)<sub>2</sub>(py)<sub>10</sub>] (BF<sub>4</sub>)<sub>2</sub> (**right**) [28]; (E) [Co<sub>8</sub>O(OH)(H<sub>2</sub>L2)<sub>6</sub>]NO<sub>3</sub> [27]; and (F) [(V<sup>V</sup>O)<sub>4</sub>(V<sup>IV</sup>O)<sub>2</sub>(O)<sub>4</sub>(L2)<sub>2</sub>(py)<sub>6</sub>] (**2**).

## 2. Results and Discussion

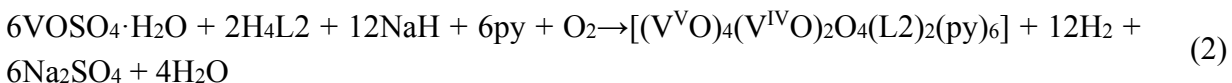
### 2.1. Synthesis

The structural versatility of H<sub>4</sub>L1 and H<sub>4</sub>L2 has been emphasized in the Introduction. The former donor has allowed the subtle control of cluster topology and nuclearity [19,40,42], whereas the latter led to the discovery of unexpected structural features [27,28]. Interestingly, all the studied compounds exhibit the ligands in a linear conformation (Scheme 1) with both coordination pockets facing the same

direction (*syn, syn* conformation). It was originally expected that vanadyl chemistry would show similar tendencies, however, the results unveil much richer and unpredictable chemistry of this ion with *bis*- $\beta$ -diketone ligands. Thus, the aerobic reaction between hydrated vanadyl sulfate and H<sub>4</sub>L1 in pyridine, in the presence of NaH, leads to the formation of the tetranuclear cluster [(VO)<sub>4</sub>(H<sub>2</sub>L1)<sub>4</sub>(py)<sub>4</sub>] (**1**). Comparing this tetrameric cluster with those already described (see below), with formula [M<sub>2</sub>(H<sub>2</sub>L1)<sub>2</sub>(S)<sub>x</sub>] (S = axial solvent ligands), which also contain partially deprotonated H<sub>2</sub>L1<sup>2-</sup> ligands occupying equatorial positions, it can be confirmed that vanadyl ions do not follow the same reactivity pattern as divalent 3d metal ions. The yield of the process suggests the possibility of other side reactions. Attempts to replicate the reaction using the product stoichiometry with the same or a different base (Et<sub>3</sub>N, TBAOH) were unsuccessful, which could indicate a potential role of Na<sup>+</sup> as a template. Possible byproducts could include oxidized vanadium(V) analogues or eventually polyoxometallate species. Despite of this, the formation of **1** may be described with a balanced chemical equation (Equation (1)):



Repetition of this reaction under the same conditions, using ligand H<sub>4</sub>L2 leads to dramatic differences in the nature of the product obtained, here consisting of a mixed valent V<sup>V</sup>V<sup>IV</sup> neutral cluster identified as [(V<sup>VO</sup>)<sub>4</sub>(V<sup>IV</sup>O)<sub>2</sub>O<sub>4</sub>(L2)<sub>2</sub>(py)<sub>6</sub>] (**2**). The incorporated O<sup>2-</sup> groups may arise from the molecules of H<sub>2</sub>O present in the reaction system. The partial oxidation of V(IV) ions in this reaction suggests that these groups originate from atmospheric oxygen, as proposed below (Equation (2)), which is very common with vanadyl ions under basic conditions in different solvents. We in fact have also observed this previously with Co(II), leading to Co<sup>III</sup>/Co<sup>II</sup> coordination systems containing the same ligand [28,43]. Besides the oxidation state of the metals, the major difference of hexanuclear cluster **2** from previously described compound **1** is the presence of fully deprotonated ligands as well as the increased metal to ligand ratio. Interestingly, the structural disparity of H<sub>4</sub>L1 vs. H<sub>4</sub>L2 products seen previously with 3d metal chemistry is maintained here (Scheme 1). However, here again, cluster **2** does not compare with any other known compound containing fully deprotonated L2<sup>4-</sup> (see below). The low yield implies also here the occurrence of side reactions. The presence of sodium ions in the reaction seems to be crucial since analogous procedures involving TBAOH as a base do not yield the same product. As well as in the case of compound **1**, it is possible that sodium ions are acting as a template in the formation of this metallamacrocyclic by stabilizing the very unusual bent conformation of the ligand (see crystal structure and SI). The net equation describing the formation of compound **2** is shown below (Equation (2)):



## 2.2. Description of Structures

### 2.1.1. [(VO)<sub>4</sub>(H<sub>2</sub>L1)<sub>4</sub>(py)<sub>4</sub>] (**1**).

Compound **1** crystallizes in the monoclinic space group *P2<sub>1</sub>/c* as a solvated neutral metallacyclophane with the formula content [(VO)<sub>4</sub>(H<sub>2</sub>L1)<sub>4</sub>(py)<sub>4</sub>]·6py (**1**·6py). The asymmetric unit is formed by one half of this formula, whereas the unit cell is composed of two full molecules. Crystallographic data are listed in Table S1, while bond distances and angles are collected in the Table S2. The cluster of **1** consists of

four vanadyl ( $\text{V}^{\text{IV}}\text{O}^{2+}$ ) ions held together by four partially deprotonated  $\text{H}_2\text{L}^{1-}$  ligands accompanied by four pyridine molecules which complete the distorted octahedral  $\text{O}_5\text{N}$  coordination environment around the metal ions (Figure 1 and Figure S1). Bond Valence Sum analysis (SI) confirms the assigned oxidation states (Table S3). The O-donors are in two different conformations and in both cases these chelate the metal centers with their two  $\beta$ -diketonato coordination pockets while keeping the phenolic protons intact. The topology of the cluster can be described as rhomboidal, resulting from the two distinct conformations of the  $\text{H}_2\text{L}^{1-}$  ligands, obtained by differing degrees of rotation around the single bonds between the central *m*-phenylene spacer and the  $\beta$ -diketone groups (with both planes either in the vicinity of  $0^\circ$  or near  $180^\circ$ ). Thus, the short side of the parallelogram ( $\text{V}\cdots\text{V}$  distance of  $7.514(3)$  Å) spans the ligand in a linear conformation where both chelating pockets are orientated in the same direction. The longer side ( $\text{V}\cdots\text{V}$  distance of  $10.892(4)$  Å) is defined by bent (V-shape)  $\text{H}_2\text{L}^{1-}$  ligands with both coordination pockets pointing to neatly different directions, in the same way as found in the crystal structure of the analogous ligand  $\text{H}_2\text{L}2$  [28]. The latter pair of ligands exhibit a nearly flat conformation and lie parallel to each other, establishing mutual intramolecular  $\pi\cdots\pi$  interactions (Figure S1). This causes the marked anisotropy of the  $[\text{V}_4]$  parallelogram (short  $\text{V}\cdots\text{V}$  diagonal distance,  $6.508(3)$  Å; long  $\text{V}\cdots\text{V}$  diagonal distance,  $17.546(5)$  Å). This also prevents the occupation of the central cavity of the assembly by any potential guest molecules (such as pyridine).

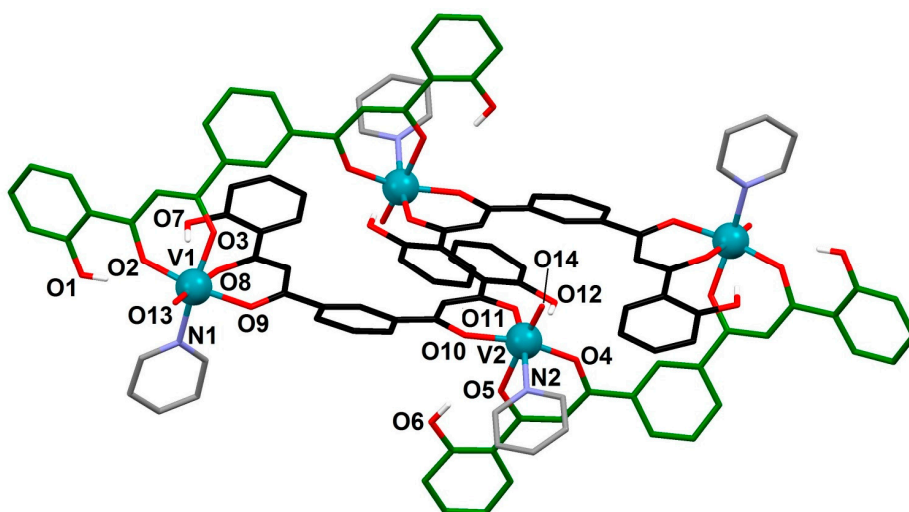


**Figure 1.** Molecular structure of  $[(\text{VO})_4(\text{H}_2\text{L})_4(\text{py})_4]$  (**1**) with crystallographically-independent heteroatoms labeled. Only phenolic hydrogen atoms are shown for clarity. Carbon atoms of each ligand conformation are black and green respectively, while these of pyridine are grey.

Both crystallographically-independent vanadium ions of **1** exhibit the *trans* effect within the axis containing the  $\text{V}=\text{O}$  bond, leading to two very disparate  $\text{V}-\text{O}$  bond distances (Table S2). The equatorial plane around the vanadium atoms is not fully homogeneous either, with three  $\text{V}-\text{O}$  bond lengths in the range of  $1.944(8)$  to  $2.011(8)$  Å, and one  $\text{V}-\text{N}$  bond of  $2.149(10)$  and  $2.142(10)$  Å for  $\text{V}1$  and  $\text{V}2$  respectively (Figure S1), while the metals are situated approximately  $0.3$  Å outside this  $\text{O}_3\text{N}$  plane towards the oxide ligand. These distortions are in agreement with the reported parameters for other vanadium compounds with the same coordination environment [44–49]. The cluster exhibits four intramolecular hydrogen bonds between phenolic  $-\text{OH}$  groups and the oxygen atoms from the adjacent

coordinated  $\beta$ -diketonato moiety (Figure S2, Table S4). The structure of **1** was analyzed for possible  $V=O \cdots C$  supramolecular contacts [50]. Indeed, the  $O \cdots C$  distance of one such contact ( $V1=O13 \cdots C51$ ;  $O \cdots C$  dist.,  $3.12(2)$  Å and  $V-O-C$  ang.,  $173.5(5)^\circ$ ) is shorter than  $3.2$  Å, considered the value of the sum of Van der Waals radii, thus contributing to link molecules into chains within the lattice. In addition, the molecules are further organized in the solid as two-dimensional sheets *via*  $\pi \cdots \pi$  stacking involving the central phenyl ring of the “linear”  $H_2L1^{2-}$  ligand or through  $C-H \cdots O$  hydrogen bonding contacts between “bent” and “linear” ligands, respectively, from neighboring molecules. The third dimension of the crystal structure is maintained through weaker interactions between sheets by means of  $C-H \cdots O$  and  $C-H \cdots \pi$  contacts (Figure S2, Table S5). The voids left between the molecules constitute channels occupied by pyridine molecules (Figure S3).

### 2.1.2. $[(V^V O)_4(V^{IV} O)_2 O_4(L2)_2(py)_6]$ (2)

Compound **2** crystallizes in the triclinic *P*-1 space group as a neutral, mixed-valent coordination cluster with the formula content  $[(V^V O)_4(V^{IV} O)_2 O_4(L2)_2(py)_6]$  (**2**· $3.44py$ ). The asymmetric unit includes half of this composition while the unit cell consists of one full solvated cluster (Table S1). Bond distances and angles are collected in Table S6. The molecular structure of **2** consists of two well-separated mixed metal  $V^V_2V^{IV}$  trinuclear units as part of a cyclic coordination cage involving two fully deprotonated *bis*- $\beta$ -diketone ligands ( $L2^{4-}$ ). The oxidation state assignments are in full agreement with BVS analysis (Supporting Information, Table S7). Each ligand binds two metals of one cluster with two metals of the other, thus keeping both aggregates separate, but together within the molecule. In doing so, the ligands exhibit a rare bent conformation (Scheme 1 and Figure 2 and Figure S4) similar to that seen in **1**, but with an asymmetric coordination mode. Thus,  $L2^{4-}$  is chelating and bridging two metals on one side via the phenoxido-diketonato moiety with a monoatomic bridge, whereas the other side chelates one metal with the  $\beta$ -diketonate and binds the other one with the phenolate moiety acting as a terminal ligand. The coordination environment around the metals is completed with three terminal pyridine molecules and two  $\mu-O^{2-}$  groups, each of the latter serving as one edge of a  $[V_3]$  triangle. The shortest side of the triangle is defined by two  $V^V$  atoms ( $d(V1 \cdots V2) = 3.125(1)$  Å), allocated within the hydroxyphenyl- $\beta$ -diketonate pocket, while the longest one corresponds to a  $V^{IV}-V^V$  pair of atoms ( $d(V1 \cdots V3) = 5.644(1)$  Å), with no direct link between them. The remaining side of the triangle measures  $3.560(1)$  Å and spans a  $V^{IV}$  ( $V3$ ) and  $V^V$  ( $V2$ ) ion through the  $\mu-O^{2-}$  bridge (Figure S5). The flexibility of the ligand enables the assembly of a metal topology with no precedents for this family of *bis*- $\beta$ -diketonate ligands. Interestingly, the distribution and orientation of oxygen and nitrogen atoms from  $L2^{4-}$  towards the cavity of the coordination cage indicates that the formation of this entity could be templated with the sodium ions (Figure S6), with its absence in the final product perhaps related to electroneutrality requirements.

The coordination environment around all three vanadium ions ranges from distorted octahedral  $O_4N_2$   $V(IV)$  and  $O_5N$   $V(V)$  to  $O_5$  square-pyramidal  $V(V)$ , corresponding to  $V3$ ,  $V1$ , and  $V2$ , respectively (Figure S5A). Atom  $V3$  exhibits an almost identical distortion as seen in **1**, with noticeable *trans* effect and differing bonds in the equatorial plane. The metal is  $0.237$  Å away of the equatorial plane. Square pyramidal  $V2$  also exhibits severe distortion at the equatorial plane ( $V-O$  bonds ranging  $1.689(3)$  to  $2.064(3)$  Å). Interestingly, the  $V2-O$  bond of the  $V^{IV}-V^V$  bridge is shorter ( $1.689(3)$  Å) than that involved in the  $V^V-V^V$  bridge ( $1.923(4)$  Å). The vanadium atom lays  $0.514$  Å outside of the equatorial plane,

towards the double-bonded oxygen atom. The octahedral environment of V1 is also much distorted, due in part to the diversity of the donors around it. The coordination numbers of the  $V^V$  sites located within the hydroxyphenyl- $\beta$ -diketonate pocket are five and six, respectively, as seen previously for the pairs of the discrete dimers reported for ligand H<sub>4</sub>L1 with other 3d metals (Figure S5) [19,42].

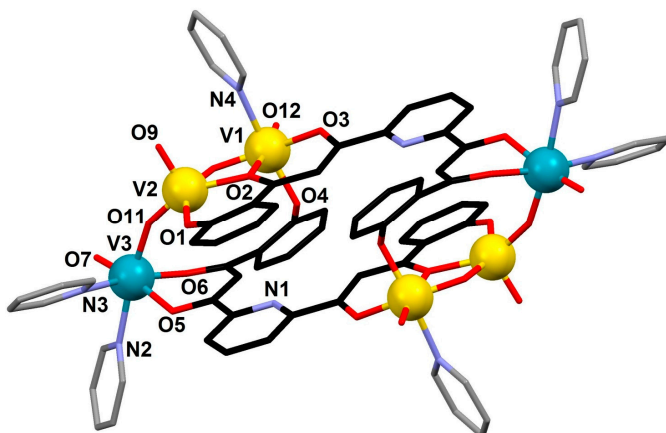


**Figure 2.** Molecular structure of  $[(V^V O)_4 (V^{\text{IV}} O)_2 (O)_4 (L_2)_2 (\text{py})_6]$  (**2**) with crystallographically-independent heteroatoms labeled. Carbon atoms of  $L_2^{2-}$  are in black while these from pyridine are grey. Vanadium(V) atoms are yellow balls, while the vanadium(IV) atoms are blue.

The clusters of **2** interact through  $V=O \cdots C$  close contacts [50] at V3, building polymeric layers supported by  $\pi \cdots \pi$  stacking contacts together with  $V=O \cdots C-H$  contacts at V2 (Figures S7 and S8, Table S8). The third dimension of the crystal structure is achieved through  $V=O \cdots H-C$  contacts between the neighboring layers (Figure S7). The network of intermolecular interactions enables gathering of ten neighboring molecules per cluster forming voids in between them for the accommodation of solvent molecules. Solvate pyridine molecules (a total of 3.44 molecules per cluster) interact weakly with the clusters via  $C-H \cdots \pi$  contacts (Figure S9).

### 2.3. Mass Spectrometry

Metallacyclophanes **1** and **2** are slightly-to-moderately soluble in THF, MeOH, and DMF allowing the assessment of their stability in solution through mass spectrometry. A very detailed analysis was then performed. Thus, positive mode MALDI-TOF spectra of **1** (Figures S10–S13) revealed the existence of the tetranuclear  $[(\text{VO})_4 (\text{H}_2\text{L}1)_4]$  core in THF solution, as well as some of its fragments like  $[(\text{VO})_4 (\text{L}1)_2]^+$ ,  $[\text{V}(\text{VO})_3 (\text{L}1)_2]^+$  and  $[\text{V}_2(\text{VO})_2 (\text{HL}1)_3 (\text{CH}_3\text{OH})]^+$ . Fragments lacking one or two of the metal ions and ligands are also observed (e.g.,  $[(\text{VO})_3 (\text{HL}1)_2]^+$ ,  $[(\text{VO})_3 (\text{HL}1)(\text{H}_2\text{L}1)]^+$ ,  $[(\text{VO})_3 (\text{HL}1)_2 (\text{H}_2\text{L}1)]^+$ ,  $[(\text{VO})_2 (\text{H}_2\text{L}1)_2]^+$ ,  $[(\text{VO})_2 (\text{H}_2\text{L}1)_2] + \text{Na}^+ (\text{K}^+)$ , and  $[\text{V}(\text{VO})(\text{H}_2\text{L}1)_2]^+$ ), as well as those including DHB in their composition (e.g.,  $[(\text{VO})_3 (\text{H}_2\text{L}1)_4 (\text{C}_6\text{H}_3(\text{OH})_2\text{COOH})]^+$ ,  $[(\text{VO})_3 (\text{H}_2\text{L}1)_3 (\text{C}_6\text{H}_3(\text{OH})_2\text{COO})_3]^+$ ,  $[(\text{VO})_3 (\text{H}_2\text{L}1)_3 (\text{C}_6\text{H}_3(\text{OH})_2\text{COO})_2]^+$ , etc.) inherent to the technique employing DHB matrix. Significant fragmentation of the compound is evident also from the existence of many monometallic fragments such as  $[\text{V}(\text{H}_2\text{L}1)]^+$ ,  $[(\text{VO})(\text{H}_3\text{L}1)]^+$ ,  $[(\text{VO}_2)(\text{H}_4\text{L}1)]^+$  where the oxidation state of vanadium varies from +3 to +5. In the negative mode of detection, polynuclear

molecular fragments with different metal to ligand ratios were found (e.g.,  $[(\text{VO})_3(\text{VO}_2)(\text{L}1)_2]^-$ ,  $[(\text{VO})_3(\text{HL}1)(\text{L}1)]^-$  and  $[(\text{VO})(\text{VO}_2)\text{L}1]^-$ ) along with mononuclear entities, such as  $[\text{V}(\text{L}1)]^-$  and  $[(\text{VO})(\text{HL}1)]^-$  (Figure S14). On the other hand, the existence of the hexanuclear core  $[(\text{VO})_6(\text{L}2)_2]$  was not observed through MALDI-TOF spectra of compound **2** (neither in positive nor negative mode) due to the significant fragmentation of the molecule (Figures S15–S17). This fact is understandable bearing in mind that the stability of this cluster decreases significantly with the loss of axial pyridine ligands as well as oxide co-ligands. In the positive mode of detection, polynuclear entities such as  $[(\text{VO})_2(\text{H}_2\text{L}2)_2] + \text{Na}^+$  and  $[(\text{VO})_3(\text{HL}2)_2] + \text{Na}^+$  are the most abundant along with the free ligand salts of sodium and potassium ( $\text{H}_4\text{L}2 + \text{Na}^+$  and  $\text{H}_4\text{L}2 + \text{K}^+$ ). Related to this, mononuclear  $[\text{V}(\text{L}2)]^-$  and  $[(\text{VO})(\text{HL}1)]^-$  moieties are dominating the negative mode MALDI-TOF spectra of this compound (as previously seen also in the case of the compound **1**) together with the appearance of dinuclear and trinuclear species (e.g.,  $[(\text{VO})_3(\text{HL}2)(\text{L}2)]^-$ ,  $[\text{V}(\text{VO})(\text{HL}2)_2]^-$ , Figure S17).

#### 2.4. Magnetic Properties

Variable temperature magnetization measurements were performed on powdered microcrystalline samples of both compounds in the 2 K to 300 K range under constant magnetic fields of 1 T and 0.5 T for **1** and **2**, respectively. In addition, magnetization measurements at 2 K in the field range of 0–5 T were performed. The resulting  $\chi_{\text{M}}T$  vs.  $T$  and  $M/N\mu_B$  vs.  $H$  curves are presented on Figures 3 and 4, respectively ( $\chi_{\text{M}}$  is the paramagnetic susceptibility per mole of V<sub>4</sub> cluster). For compound **1**, the value of  $\chi_{\text{M}}T$  at 300 K is  $1.58 \text{ cm}^3 \cdot \text{K} \cdot \text{mol}^{-1}$ , only slightly above the expected number for four uncoupled  $S = 1/2$  spin centers with  $g = 2$  ( $1.500 \text{ cm}^3 \cdot \text{K} \cdot \text{mol}^{-1}$ ). This is consistent with the postulated oxidation state of the metal centers for this cluster (V<sup>IV</sup>). The  $\chi_{\text{M}}T$  value remains then constant upon cooling and only rises very slightly near 15 K to reach a maximum of  $1.60 \text{ cm}^3 \cdot \text{K} \cdot \text{mol}^{-1}$  at 10 K before declining more sharply down to a value of  $1.48 \text{ cm}^3 \cdot \text{K} \cdot \text{mol}^{-1}$  at 2 K. This behavior shows that the paramagnetic centers within the cluster remain only very weakly coupled. The extent of this coupling was determined by fitting the experimental data using an iterative matrix diagonalization procedure with the program PHI [51], employing as model Hamiltonian that in Equation (3).

$$\hat{H} = -2J(\hat{S}_1\hat{S}_2 + \hat{S}_3\hat{S}_4) - 2J'(\hat{S}_1\hat{S}_3 + \hat{S}_2\hat{S}_4) \quad (3)$$

The coupling scheme used to build this Hamiltonian is that of Scheme 2. The labels 1 to 4 refer to four different V(IV) centers numbered consecutively along the periphery of the metallacycle, but do not allow to discern which edge is  $J$  and which is  $J'$ . The fitting indeed produces very weak coupling constants ( $J = 0.51 \text{ cm}^{-1}$  and  $J' = -0.31 \text{ cm}^{-1}$ ) together with parameters  $g = 2.04$  and an additional contribution from intermolecular interactions modeled as  $zJ = 0.02 \text{ cm}^{-1}$ . Since the coupling is so weak, the values may be strongly affected by small errors, thus, only the fact that the numbers are very small must be retained from this fitting. The excellent fitting of magnetization at constant temperature (2 K) and variable magnetic field (Figure 4) confirms the results from the variable temperature magnetic susceptibility measurements, since both sets of data were fitted simultaneously.

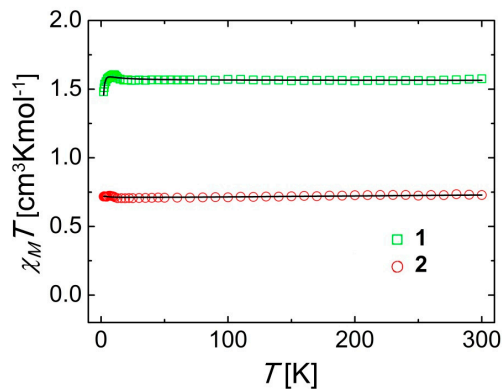


**Figure 3.**  $\chi_M T$  vs.  $T$  plots per mole of compounds **1** (green squares) and **2** (red circles). The solid lines are fits to the experimental data (see text for details).

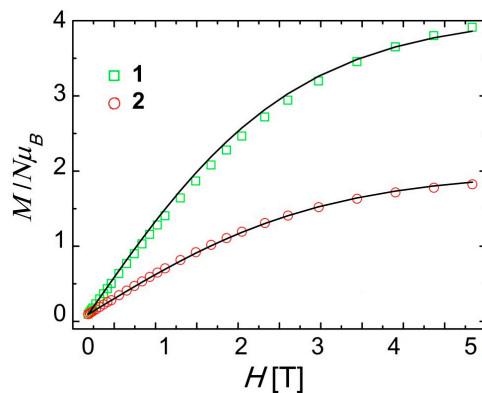
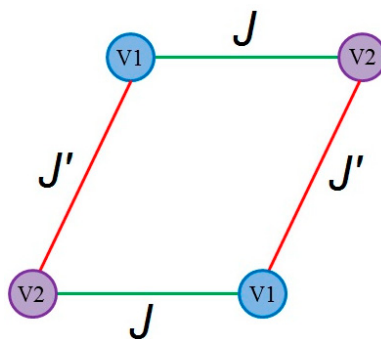


**Figure 4.**  $M/N\mu_B$  vs.  $H$  plots per mole of compounds **1** (green squares) and **2** (red circles). The solid lines are fits to the experimental data (see text for details).



**Scheme 2.** Coupling scheme employed in the Hamiltonian of Equation (3).

Hexanuclear cluster **2** contains only two V<sup>IV</sup> paramagnetic metal centres ( $S = 1/2$ ) while the remaining four metal ions are diamagnetic vanadium(V) ( $S = 0$ ). The intramolecular distance between both spin carriers is 14.679(1) Å while the shortest intermolecular distance is 5.437(1) Å. The  $\chi_M T$  product at 300 K ( $0.730 \text{ cm}^3 \cdot \text{K} \cdot \text{mol}^{-1}$ ) is slightly below the expected value ( $0.750 \text{ cm}^3 \cdot \text{K} \cdot \text{mol}^{-1}$  for  $g = 2.0$ ) for two uncoupled ( $S = 1/2$ ) vanadium(IV) centers. The value stays practically constant over the whole thermal range. Simultaneous analysis of the experimental  $\chi_M T$  vs.  $T$  and  $M/N\mu_B$  vs.  $H$  curves data using the program PHI [51], allowed fitting these data for a  $g$  value of 1.94 and with the presence of very weak

intermolecular interactions ( $zJ = 0.03 \text{ cm}^{-1}$ ) as well as temperature independent paramagnetism ( $\text{TIP} = 70 \times 10^{-6} \text{ cm}^3 \cdot \text{K} \cdot \text{mol}^{-1}$ ).

Solid state powder EPR spectra of both compounds (Figure 5) at various temperatures (5–298 K for compound **1** and 5–95 K for compound **2**) showed in each case a strong and broad isotropic resonance centered at a  $g = 1.989$  and  $g = 1.991$  for **1** and **2** respectively. These  $g$  factors are smaller than the theoretical  $g$  value of the free electron (2.0023) and are in excellent agreement with the literature reported studies of vanadyl-based systems [49,52]. On the other hand, the small discrepancies with the values obtained from fitting the magnetization data are due to the fact that the latter are from using a collective bulk thermodynamic quantity, subject to experimental errors, such as the accuracy on the molecular mass, which is not the case for the EPR results, which are spectroscopic. No hyperfine coupling was observed with the  $^{51}\text{V}$  nuclei.

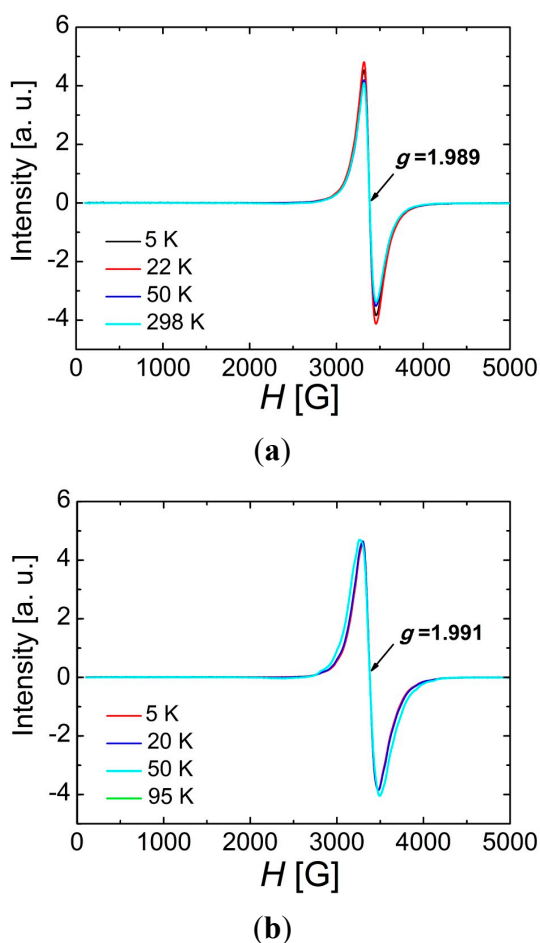


**Figure 5.** Variable temperature X-band EPR spectra on solid powdered samples of complexes **1** (a) and **2** (b).

### 3. Experimental Section

#### 3.1. Synthesis

The ligands *1,3-bis-(3-oxo-3-(2-hydroxyphenyl)-propionyl)-benzene* ( $\text{H}_4\text{L}1$ ) [40] and *1,3-bis-(3-oxo-3-(2-hydroxyphenyl)-propionyl)-pyridine* ( $\text{H}_4\text{L}2$ ) [41] were prepared according to a slightly

modified procedure published by us where the solvent of the reaction was changed from DME to dry THF. Solvents and reagents were used as received without purification. Sodium hydride was used as 60% suspension in mineral oil while vanadyl sulfate was used as monohydrate salt ( $\text{VOSO}_4 \cdot \text{H}_2\text{O}$ ).

### 3.1.1. Synthesis of $[(\text{VO})_4(\text{H}_2\text{L})_4(\text{py})_4]$ (**1**)

Solid NaH (11.9 mg, 0.298 mmol) was added to the yellow solution of ligand H<sub>4</sub>L1 (30.0 mg, 0.075 mmol) in pyridine (10 mL) causing immediate hydrogen evolution and the change of color of the solution to light orange. The mixture was stirred at room temperature for 10 min and it was then added dropwise to a hot solution of  $\text{VOSO}_4 \cdot \text{H}_2\text{O}$  (27.0 mg, 0.149 mmol) in pyridine (10 mL) changing its color from blue to orange. The resulting reaction mixture was stirred at room temperature for 90 min and then filtered to remove a very small amount of brown precipitate (less than 3 mg). The remaining filtrate was layered with hexanes, diethyl ether, or toluene, producing very thin yellow-orange plates within a week with an average yield of 37% (18.4 mg). Prior to any analysis, crystals were washed with water and toluene to remove traces of any residual salts ( $\text{Na}_2\text{SO}_4$ ) and impurities. IR (KBr pellet: 0.9 mg sample + 99.6 mg KBr, Figure S18):  $\nu/\text{cm}^{-1}$ : 3440 m, 1620 m, 1518 s, 1338 m, 1299 m, 1198 m, 959 m, 760 m, 698 m. EA (%); Calc. (Found for **1**·2.65H<sub>2</sub>O·1.45toluene): C 64.01 (64.04), H 4.30 (4.26), N 2.37 (2.33).

### 3.1.2. Synthesis of $[(\text{V}^{\text{V}}\text{O})_4(\text{V}^{\text{IV}}\text{O})_2(\text{O})_4(\text{L}2)_2(\text{py})_6] \cdot (\textbf{2})$

Solid NaH (11.9 mg, 0.298 mmol) was added to a yellow solution of ligand H<sub>4</sub>L2 (30.0 mg, 0.074 mmol) in pyridine (10 mL) causing immediate hydrogen evolution and the change of color of the solution to yellow-orange. The mixture was stirred at room temperature for 10 min and afterwards it was added dropwise to a hot solution of  $\text{VOSO}_4 \cdot \text{H}_2\text{O}$  (27.0 mg, 0.149 mmol) in pyridine (10 mL) changing its color from blue to orange-brown. The resulting reaction mixture was stirred at room temperature for 90 min and then filtered. A very small amount of dark brown precipitate was removed (about 4 mg) by filtration. The filtrate was layered with toluene causing the formation of small dark orange plates within a week with an average yield of 29% (21.6 mg). Prior to any analysis, crystals were washed with water and toluene to remove traces of any residual salts ( $\text{Na}_2\text{SO}_4$ ) and impurities. IR (KBr pellet: 1.1 mg sample + 115.6 mg KBr, Figure S19):  $\nu/\text{cm}^{-1}$ : 3424 m, 1605 m, 1525 s, 1444 m, 1345 m, 1251 m, 1215 m, 1070 m, 964 m, 952 m, 826 m, 765 m, 740 m, 694 m. EA (%); Calc. (Found for **2**·2H<sub>2</sub>O·1.3toluene): C 53.94 (53.90), H 3.74 (3.60), N 5.91 (5.78).

## 3.2. X-Ray Crystallography

Data for **1** were collected on a yellow plate at 100 K with a Bruker (Madison, WI, USA) APEX II CCD diffractometer on the Advanced Light Source beamline 11.3.1 at Lawrence Berkeley National Laboratory, from a silicon 111 monochromator ( $\lambda = 0.7749 \text{ \AA}$ ). Data for **2** were collected at 100 K on Bruker (Madison, WI, USA) APEX II QUAZAR diffractometer equipped with a microfocus multilayer monochromator with Mo K $\alpha$  radiation ( $\lambda = 0.71073 \text{ \AA}$ ). Data reduction and absorption corrections in both cases were performed with SAINT and SADABS, respectively [53,54]. The structures were solved with direct methods and refined on  $F^2$  with SHELX-TL suite [55,56]. Very thin and fragile crystals of

compound **1** with disordered lattice solvent area showed significant diffraction only up to 1.05 Å even using synchrotron radiation (data were cut at 1.01 Å). Non-hydrogen atoms were refined anisotropically while hydrogen atoms were placed geometrically on their carrier atom and refined using suitable riding model. Disordered lattice pyridine molecules were refined over two positions using a rough rigid body restraint (AFX 66) giving the final values of relative occupancies of 0.72/0.28, 0.64/0.36, and 0.61/0.39 for pairs of disordered pyridine molecules (N1S/N4S, N2S/N5S, and N3S/N6S, respectively). The corresponding atoms were refined isotropically with a common isotropic thermal factor for each pair of pyridine molecules. An additional attempt was made to refine small disorder of one of the vanadium atoms (V2) over two positions but the model did not improve significantly and did not provide any additional information. Thus, the concerned vanadium atom was left at full occupancy and it was refined with displacement parameter restraints. Possibly related to this disorder, as well as with the poor diffraction, a number of oxygen and carbon atoms from the ligands also showed some disorder and, therefore, those atoms were refined with displacement parameters restraints. Crystals of compound **2** showed significant decrease of diffraction at resolutions better than 0.95 Å; thus, the obtained data were cut at 0.91 Å. All non-hydrogen atoms were refined anisotropically while the hydrogen atoms were placed geometrically on their carrier atoms and refined using suitable riding model. The lattice solvent area is occupied by highly disordered pyridine molecules which were refined over three positions using rigid body restraint (AFX 66) and displacement parameters restraints. Their relative occupancies were first refined and later fixed in the final refinement cycle at the converged values summing 3.44 molecules per formula unit. At the end of refinement, one residual electron density peak remained close to one of the disordered partial lattice pyridine molecules likely corresponding to some unresolved disorder. All crystallographic details can be found in CCDCs 1430322–1430323 (for **1–2**, respectively). These data can be obtained free of charge from The Cambridge Crystallographic Data Centre via [www.ccdc.cam.ac.uk/data\\_request/cif](http://www.ccdc.cam.ac.uk/data_request/cif).

### 3.3. Physical Measurements

Variable-temperature magnetic susceptibility data were obtained with a Quantum Design (San Diego, CA, USA) MPMS5 SQUID magnetometer at the “Unitat de Mesures Magnètiques” of the Universitat de Barcelona. For complex **1**, a correction for the diamagnetic contribution from the sample holder and the sample was made using the value  $\chi_{\text{dia}} = -412 \times 10^{-6} \text{ cm}^3 \cdot \text{mol}^{-1}$ , obtained from a linear regression of the linear part of the  $\chi T$  vs.  $T$  curve. For **2**, Pascal’s constants and a standard correction for the sample holder were sufficient. The results of SQUID measurements ( $\chi M T$  vs.  $T$  curve and  $M/N_{\mu B}$  vs.  $H$ ) were fitted using the program PHI [51]. X-Band EPR spectra (9.42 GHz) of powdered samples were determined on a Bruker (Madison, WI, USA) ESP300E spectrometer, with a liquid helium cryostat in the temperature range between 5 K and 300 K. The sweep width was 5000 G with the center field of 2605 G and resolution of 1024 points (4.885 G) while the used power was 0.2514 mW. Obtained spectra were processed with WINEPR Bruker software (version 2.11.0.0) (Bruker-Franzen Analytic GmbH, Rheinstetten, Germany, 1996). IR spectra were recorded as KBr pellets, in the range 4000–400  $\text{cm}^{-1}$ , with a Nicolet 5700 FT-IR spectrometer (Nicolet, Waltham, MA, USA). Elemental analyses were performed at Scientific and Technological Centers of the University of Barcelona using an elemental organic analyzer Thermo EA Flash 2000 (Thermo Fisher, Bremen, Germany) working in standard

conditions recommended by the supplier of the instrument (helium flow 140 mL/min, combustion furnace at 950 °C, chromatographic column oven at 65 °C). Mass spectra of the compounds were obtained using MALDI-TOF technique in the reflector mode on the 4800 Plus MALDI TOF/TOF (ABSciex-2010, Framingham, MA, USA) instrument equipped with Nd:YAG solid state laser (355 nm, frequency 200 Hz, pulse 3–7 ns). Molecular ions were studied in both positive and negative mode on the THF and MeOH solutions of the compounds. Analyses were carried out using different conditions: solution of the compound without any matrix, solution of the compound and the saturated matrix of the DHB (2,5-dihydroxybenzoic acid) in acetonitrile (1:1 volume ratio) or solution of the compound with the matrix containing dichloromethane solution of DCTB (10 mg/mL; *trans*-2-[3-(4-*tert*-butylphenyl)-2-methyl-2-propenylidene]malononitrile (1:1 volume ratio). In the last two cases, a mixture of sample and matrix solution was spotted on the sample plate and left to dry before the analysis by MALDI-TOF.

#### 4. Conclusions

Reactions of vanadyl sulfate with multidentate ligands H<sub>4</sub>L1 and H<sub>4</sub>L2 under strong basic conditions yielded two different neutral coordination entities,  $[(V^{IV}O)_4(H_2L1)_4(py)_4]$  (**1**) and  $[(V^V O)_4(V^{IV}O)_2(O)_4(L2)_2(py)_6]$  (**2**). To the best of our knowledge, the structural features and nuclearity of these compounds convert them into the most complex metallamacrocycles from vanadium-*bis*-β-diketone family known to date. The conformational flexibility and coordination diversity of those systems has not been observed in any of the previously prepared complexes of these ligands, using different 3d metals. This could be related to particular supramolecular features inherent to the V=O moiety. In addition to this, it is suggested that the presence of sodium ions can serve as a template in the formation of compound **2** by shaping a very peculiarly bent conformation of the ligand. In view of this versatility, the use of poly-β-diketones appears as a good alternative to isolate molecular clusters with the appropriate topologies to exploit the promising properties of V(IV) as a potential spin-based qubit. In addition, the crystal-field energy effects detected in the structure of this complex could be exploited for the design of novel heterometallic systems.

#### Acknowledgments

Guillem Aromí thanks the Generalitat de Catalunya for the prize ICREA Academia 2008 and 2013, for excellence in research and the ERC (European Research Council) for a Starting Grant (258060 FuncMolQIP). The authors thank the Spanish MICINN for funding through CTQ2009-06959 (Guillem Aromí, Ivana Borilovic) and MAT2011-24284 (Olivier Roubeau). Ivana Borilovic thanks the Generalitat de Catalunya for a Ph.D. Grant (FI-DGR 2014). Data for compound **1** were collected through access to ALS beamline 11.3.1. The Advanced Light Source is supported by the Director, Office of Science, Office of Basic Energy Sciences of the U.S. Department of Energy under contract No. DE-AC02-05CH11231.

#### Author Contributions

Ivana Borilovic conducted the synthesis and physical measurements, interpreted the data and wrote part of the paper. Olivier Roubeau collected crystallographic data, performed structure refinements and

edited the paper. Irene Fernández Vidal performed mass spectrometry measurements and interpreted the data. Simon J. Teat collected crystallographic data and performed structure refinements. Guillem Aromí planned and coordinated the research, interpreted the results and wrote part of the paper.

## Conflicts of Interest

The authors declare no conflict of interest.

## References

1. Aromí, G.; Brechin, E. Synthesis of 3d Metallic Single-Molecule Magnets. In *Single-Molecule Magnets and Related Phenomena*; Winpenny, R., Ed.; Springer: Berlin, Germany, 2006; Volume 122, pp. 1–67.
2. Layfield, R.A. Organometallic Single-Molecule Magnets. *Organometallics* **2014**, *33*, 1084–1099.
3. Rosado Piquer, L.; Sañudo, E.C. Heterometallic 3d-4f single-molecule magnets. *Dalton Trans.* **2015**, *44*, 8771–8780.
4. Woodruff, D.N.; Winpenny, R.E.P.; Layfield, R.A. Lanthanide Single-Molecule Magnets. *Chem. Rev.* **2013**, *113*, 5110–5148.
5. Sessoli, R.; Tsai, H.L.; Schake, A.R.; Wang, S.Y.; Vincent, J.B.; Folting, K.; Gatteschi, D.; Christou, G.; Hendrickson, D.N. High-Spin Molecules:  $[\text{Mn}_{12}\text{O}_{12}(\text{O}_2\text{CR})_{16}(\text{H}_2\text{O})_4]$ . *J. Am. Chem. Soc.* **1993**, *115*, 1804–1816.
6. Bousseksou, A.; Molnar, G.; Salmon, L.; Nicolazzi, W. Molecular spin crossover phenomenon: Recent achievements and prospects. *Chem. Soc. Rev.* **2011**, *40*, 3313–3335.
7. Craig, G.A.; Roubeau, O.; Aromí, G. Spin state switching in 2,6-bis(pyrazol-3-yl)pyridine (3-bpp) based Fe(II) complexes. *Coord. Chem. Rev.* **2014**, *269*, 13–31.
8. Murray, K.S. The Development of Spin-Crossover Research. In *Spin-Crossover Materials*; John Wiley & Sons Ltd: Oxford, UK, 2013; pp. 1–54.
9. Aguilà, D.; Barrios, L.A.; Velasco, V.; Roubeau, O.; Repollés, A.; Alonso, P.J.; Sesé, J.; Teat, S.J.; Luis, F.; Aromí, G. Heterodimetallic  $[\text{LnLn}']$  Lanthanide Complexes: Toward a Chemical Design of Two-Qubit Molecular Spin Quantum Gates. *J. Am. Chem. Soc.* **2014**, *136*, 14215–14222.
10. Aromí, G.; Aguilà, D.; Gamez, P.; Luis, F.; Roubeau, O. Design of magnetic coordination complexes for quantum computing. *Chem. Soc. Rev.* **2012**, *41*, 537–546.
11. Timco, G.A.; Faust, T.B.; Tuna, F.; Winpenny, R.E.P. Linking heterometallic rings for quantum information processing and amusement. *Chem. Soc. Rev.* **2011**, *40*, 3067–3075.
12. Clemente-Juan, J.M.; Coronado, E.; Gaita-Arino, A. Magnetic polyoxometalates: From molecular magnetism to molecular spintronics and quantum computing. *Chem. Soc. Rev.* **2012**, *41*, 7464–7478.
13. Aromí, G.; Gamez, P.; Reedijk, J. Poly beta-diketones: Prime ligands to generate supramolecular metalloclusters. *Coord. Chem. Rev.* **2008**, *252*, 964–989.
14. Grillo, A.V.; Seddon, J.E.; Grant, M.C.; Aromí, G.; Bollinger, C.J.; Folting, K.; Christou, G. Bis( $\beta$ -diketonate) ligands for the synthesis of bimetallic complexes of Ti<sup>III</sup>, V<sup>III</sup>, Mn<sup>III</sup> and Fe<sup>III</sup> with a triple-helix structure. *Chem. Commun.* **1997**, 1561–1562.

15. Li, H.-F.; Yan, P.-F.; Chen, P.; Wang, Y.; Xu, H.; Li, G.-M. Highly luminescent bis-diketone lanthanide complexes with triple-stranded dinuclear structure. *Dalton Trans.* **2012**, *41*, 900–907.
16. Saalfrank, R.W.; Maid, H.; Scheurer, A. Supramolecular Coordination Chemistry: The Synergistic Effect of Serendipity and Rational Design. *Angew. Chem. Int. Ed.* **2008**, *47*, 8794–8824.
17. Aguila, D.; Barrios, L.A.; Roubeau, O.; Teat, S.J.; Aromí, G. Molecular assembly of two [Co(II)<sub>4</sub>] linear arrays. *Chem. Commun.* **2011**, *47*, 707–709.
18. Clegg, J.K.; Li, F.; Lindoy, L.F. Di-, tri- and oligometallic platforms: Versatile components for use in metallo-supramolecular chemistry. *Coord. Chem. Rev.* **2013**, *257*, 2536–2550.
19. Barrios, L.A.; Aguilà, D.; Roubeau, O.; Gamez, P.; Ribas-Ariño, J.; Teat, S.J.; Aromí, G. Designed Topology and Site-Selective Metal Composition in Tetranuclear [MM'···M'M] Linear Complexes. *Chem. A Eur. J.* **2009**, *15*, 11235–11243.
20. Li, F.; Clegg, J.K.; Jensen, P.; Fisher, K.; Lindoy, L.F.; Meehan, G.V.; Moubaraki, B.; Murray, K.S. Predesigned Hexanuclear CuII and CuII/NiII Metallacycles Featuring Six-Node Metallaconorand Structural Motifs. *Angew. Chem. Int. Ed.* **2009**, *48*, 7059–7063.
21. Cherutoi, J.K.; Sandifer, J.D.; Pokharel, U.R.; Fronczek, F.R.; Pakhomova, S.; Maverick, A.W. Externally and Internally Functionalized Copper(II)  $\beta$ -Diketonate Molecular Squares. *Inorg. Chem.* **2015**, *54*, 7791–7802.
22. Bonitatebus, J.P., Jr.; Mandal, K.S. Synthesis and crystal structures of low-valent binuclear vanadium complexes using the tethering ligand *m*-xylylenebis(acetylacetone) (*m*-xba<sup>2-</sup>). *Chem. Commun.* **1998**, 939–940.
23. Saalfrank, R.W.; Löw, N.; Kareth, S.; Seitz, V.; Hampel, F.; Stalke, D.; Teichert, M. Crown Ethers, Double-Decker, and Sandwich Complexes: Cation-Mediated Formation of Metallatopomer Coronates. *Angew. Chem. Int. Ed.* **1998**, *37*, 172–175.
24. Zhang, Y.; Wang, S.; Enright, G.D.; Breeze, S.R. Tetraacetyleneethane Dianion (Tae) as a Bridging Ligand for Molecular Square Complexes: Co<sup>II</sup><sub>4</sub>(Tae)<sub>4</sub>(Dpa)<sub>4</sub>, Dpa = Di-2-pyridylamine, a Chiral Molecular Square in the Solid State. *J. Am. Chem. Soc.* **1998**, *120*, 9398–9399.
25. Aromí, G.; Ribas, J.; Gamez, P.; Roubeau, O.; Kooijman, H.; Spek, A.L.; Teat, S.; MacLean, E.; Stoeckli-Evans, H.; Reedijk, J. Aggregation of [Cu<sup>II</sup><sub>4</sub>] Building Blocks into [Cu<sup>II</sup><sub>8</sub>] Clusters or a [Cu<sup>II</sup><sub>4</sub>]<sub>∞</sub> Chain through Subtle Chemical Control. *Chem. A Eur. J.* **2004**, *10*, 6476–6488.
26. Saalfrank, R.W.; Löw, N.; Demleitner, B.; Stalke, D.; Teichert, M. Metal-Directed Formation of Tetra-, Hexa-, Octa-, and Nonanuclear Complexes of Magnesium, Calcium, Manganese, Copper, and Cadmium. *Chem. A Eur. J.* **1998**, *4*, 1305–1311.
27. Salinas-Uber, J.; Barrios, L.A.; Roubeau, O.; Aromí, G. A novel *bis*- $\beta$ -diketonate ligand stabilizes a [Co(II)<sub>8</sub>] cage that encapsulates a ( $\mu_3$ -O)···H···( $\mu_3$ -O) moiety. *Polyhedron* **2013**, *54*, 8–12.
28. Velasco, V.; Aguila, D.; Barrios, L.A.; Borilovic, I.; Roubeau, O.; Ribas-Arino, J.; Fumanal, M.; Teat, S.J.; Aromí, G. New coordination features; a bridging pyridine and the forced shortest non-covalent distance between two CO<sub>3</sub><sup>2-</sup> species. *Chem. Sci.* **2015**, *6*, 123–131.
29. Kioseoglou, E.; Petanidis, S.; Gabriel, C.; Salifoglou, A. The chemistry and biology of vanadium compounds in cancer therapeutics. *Coord. Chem. Rev.* **2015**, *301–302*, 87–105.
30. Pessoa, C.J.; Garribba, E.; Santos, M.F.A.; Santos-Silva, T. Vanadium and proteins: Uptake, transport, structure, activity and function. *Coord. Chem. Rev.* **2015**, *301–302*, 49–86.

31. Yoshikawa, Y.; Sakurai, H.; Crans, D.C.; Micera, G.; Garribba, E. Structural and redox requirements for the action of anti-diabetic vanadium compounds. *Dalton Trans.* **2014**, *43*, 6965–6972.
32. Rehder, D. The Bioinorganic Chemistry of Vanadium. *Angew. Chem. Int. Ed.* **1991**, *30*, 148–167.
33. Sutradhar, M.; Martins, L.M.D.R.S.; da Silva, G.M.F.C.; Pombeiro, A.J.L. Vanadium complexes: Recent progress in oxidation catalysis. *Coord. Chem. Rev.* **2015**, *301–302*, 200–239.
34. Amadio, E.; di Lorenzo, R.; Zonta, C.; Licini, G. Vanadium catalyzed aerobic carbon–carbon cleavage. *Coord. Chem. Rev.* **2015**, *301–302*, 147–162.
35. Chen, L.; Jiang, F.-L.; Su, W.-P.; Yue, C.-Y.; Yuan, D.-Q.; Hong, M.-C. A dinuclear vanadium compound with 24-membered macrocycle generated via formation of S–C bonds. *Inorganica Chimica Acta* **2009**, *362*, 407–413.
36. Clegg, J.K.; Kim, Y.; Lindoy, L.F. Discrete and polymeric supramolecular architectures derived from dinuclear oxovanadium(IV) complexes of aryl-linked bis-diketonato ligands and nitrogen donor co-ligands. *J. Incl. Phenom. Macrocycl. Chem.* **2015**, *82*, 247–257.
37. Castro, S.L.; Sun, Z.; Grant, C.M.; Bollinger, J.C.; Hendrickson, D.N.; Christou, G. Single-Molecule Magnets: Tetranuclear Vanadium(III) Complexes with a Butterfly Structure and an  $S = 3$  Ground State. *J. Am. Chem. Soc.* **1998**, *120*, 2365–2375.
38. Bertaina, S.; Gambarelli, S.; Mitra, T.; Tsukerblat, B.; Muller, A.; Barbara, B. Quantum oscillations in a molecular magnet. *Nature* **2008**, *453*, 203–207.
39. Zadrozny, J.M.; Niklas, J.; Poluektov, O.G.; Freedman, D.E. Multiple Quantum Coherences from Hyperfine Transitions in a Vanadium(IV) Complex. *J. Am. Chem. Soc.* **2014**, *136*, 15841–15844.
40. Aromí, G.; Boldron, C.; Gamez, P.; Roubeau, O.; Kooijman, H.; Spek, A.L.; Stoeckli-Evans, H.; Ribas, J.; Reedijk, J. Complexes of a novel multinucleating poly- $\beta$ -diketonate ligand. *Dalton Trans.* **2004**, 3586–3592.
41. Craig, G.A.; Barrios, L.A.; Costa, J.S.; Roubeau, O.; Ruiz, E.; Teat, S.J.; Wilson, C.C.; Thomas, L.; Aromí, G. Synthesis of a novel heptacoordinated Fe(iii) dinuclear complex: Experimental and theoretical study of the magnetic properties. *Dalton Trans.* **2010**, *39*, 4874–4881.
42. Barrios, L.A.; Aguilà, D.; Méllat, S.; Roubeau, O.; Teat, S.J.; Gamez, P.; Aromí, G. Synthesis and properties of a novel linear [Ni<sub>4</sub>L<sub>2</sub>(py)<sub>6</sub>] cluster: Designed ligand-controlled topology of the metals. *C. R. Chim.* **2008**, *11*, 1117–1120.
43. Grybo, R.; Samotus, A.; Popova, N.; Bogolitsyn, K. Kinetics of oxidation of vanadyl acetylacetone by oxygen in methanolic solution. *Transit. Met. Chem.* **1997**, *22*, 61–64.
44. Carofiglio, T.; Solari, E.; Floriani, C.; Chiesi-Villa, A.; Rizzoli, C. UV stabilizers bonded to transition metals: Synthesis and X-ray structure of 2-(2'-hydroxyphenyl)benzotriazole-oxovanadium(IV) and -dioxiomolybdenum(VI) complexes. *Polyhedron* **1996**, *15*, 4435–4440.
45. Ishida, T.; Mitsubori, S.-I.; Nogami, T.; Takeda, N.; Ishikawa, M.; Iwamura, H. Ferromagnetic Exchange Coupling of Vanadium(IV) d $\pi$  Spins across Pyrimidine Rings: Dinuclear Complexes of Oxovanadium(IV) Bis(1,1,1,5,5-hexafluoropentane-2,4-dionate) Bridged by Pyrimidine Derivatives. *Inorg. Chem.* **2001**, *40*, 7059–7064.
46. Kadirova, Z.C.; Rahmonova, D.S.; Talipov, S.A.; Ashurov, J.M.; Parpiev, N.A. Bis(acetylacetonato- $\kappa^2O,O'$ )(2-amino-1-methyl-1H-benzimidazole- $\kappa^3N^3$ )oxidovanadium(IV). *Acta Crystallogr. Sect. E* **2009**, *65*, m819.

47. Lobana, T.S.; Kinoshita, I.; Kimura, K.; Nishioka, T.; Shiomi, D.; Isobe, K. Pyridine-2-sulfonates as Versatile Ligands for the Synthesis of Novel Coordinative and Hydrogen-Bonded Supramolecules. *Eur. J. Inorg. Chem.* **2004**, *2004*, 356–367.
48. Mestrovic, E.; Bucar, D.-K.; Halasz, I.; Stilinovic, V. The first adduct of bis(1,3-diphenyl-1,3-propanedionato)oxovanadium(IV). *Acta Crystallogr. Sect. E* **2004**, *60*, m1920–m1922.
49. Smith, T.S.; Root, C.A.; Kampf, J.W.; Rasmussen, P.G.; Pecoraro, V.L. Reevaluation of the Additivity Relationship for Vanadyl-Imidazole Complexes: Correlation of the EPR Hyperfine Constant with Ring Orientation. *J. Am. Chem. Soc.* **2000**, *122*, 767–775.
50. Stilinovic, V.; Bucar, D.-K.; Halasz, I.; Mestrovic, E. V=O···C interactions in crystal structures of oxovanadium-coordination compounds. *New J. Chem.* **2013**, *37*, 619–623.
51. Chilton, N.F.; Anderson, R.P.; Turner, L.D.; Soncini, A.; Murray, K.S. PHI: A powerful new program for the analysis of anisotropic monomeric and exchange-coupled polynuclear d- and f-block complexes. *J. Comput. Chem.* **2013**, *34*, 1164–1175.
52. Smith II, T.S.; LoBrutto, R.; Pecoraro, V.L. Paramagnetic spectroscopy of vanadyl complexes and its applications to biological systems. *Coord. Chem. Rev.* **2002**, *228*, 1–18.
53. SAINT, version V8.32B; Bruker AXS Inc.: Madison, WI, USA, 2012.
54. SADABS, version 2012/1; Bruker AXS Inc.: Madison, WI, USA, 2012.
55. Sheldrick, G.M. SHELXTL, version 2014; Bruker AXS Inc.: Madison, WI, USA, 2014.
56. Sheldrick, G. Crystal structure refinement with SHELXL. *Acta Crystallogr. Sect. C* **2015**, *71*, 3–8.

© 2015 by the authors; licensee MDPI, Basel, Switzerland. This article is an open access article distributed under the terms and conditions of the Creative Commons Attribution license (<http://creativecommons.org/licenses/by/4.0/>).